Coaggregation of Two Anionic Azo Dyestuffs: A Combined Static Light Scattering and X-Ray Scattering Study

Rolf Michels,[†] Günter Goerigk,[‡] Ulla Vainio,[‼] Jérémie Gummel,[§] and Klaus Huber*[,†]

[†]Universität Paderborn, Department für Physikalische Chemie, Warburger Straße 100, D-33098 Paderborn, Germany
[‡]Helmholtz-Zentrum Berlin, Institut Weiche Materie und Funktionale Materialien, Hahn-Meitner-Platz 1, D-14109 Berlin, Germany
[‼]Deutsches Elektronen-Synchrotron DESY, Notkestraße 85, D-22607 Hamburg, Germany
[§]Procter & Gamble Technical Centre, Whitley Road, Longbenton, Newcastle Upon Tyne, Tyne And Wear, NE12 9SR, United Kingdom
*to whom correspondence should be addressed
E-mail: klaus.huber@upb.de
Phone: +49 5251 602125

Supporting Information

SUPPORTING INFORMATION. Reproducibility of Aggregation Experiments; Modeling of Small-Angle Scattering Data by Means of the Cylinder Model; Cylinder Radii Obtained from Guinier Fits; Parameter Distortion Based on an Interpretation of the Scattering of a Mixture of Small and Large Cylinders by Means of the Form Factors of Large Cylinders; Estimation of the Dyestuff Concentration within Centrifuged Dyestuff Gels; Calculation of Sr^{2+} Concentrations from X-Ray Absorption Spectra; Direct Comparison of the SAXS from Samples Used for SAXS and ASAXS Experiments. This material is available free of charge via the Internet at http://pubs.acs.org.

Reproducibility of Aggregation Experiments

The reproducibility of dyestuff aggregation experiments is exemplified in Figures S1 and S2. Figure S1 demonstrates that an initiation by hand mixing and an initiation by using a stopped-flow device lead to growth processes that are not distinguishable from each other. In Figure S2, two features are demonstrated. First, different shots with the stopped-flow device lead to growth processes that are equal within the uncertainty of the SAXS data. Second, data sets that are recorded at equal times after initiation but at different sample-to-detector distances exhibit equal intensities within their overlapping q regime and thus can be merged without difficulty.

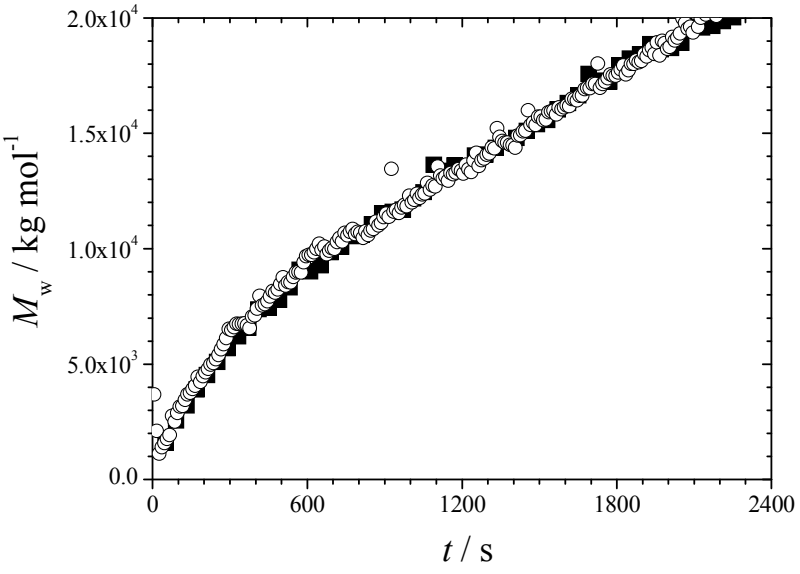

Figure S1. The evolution of the weight-averaged molar mass M_w is compared for two mixing cycles during which equal volumes of an aqueous magnesium chloride solution and an aqueous solution of RD and YD with a molar ratio of 1:1 were combined at time $t = 0$. Both mixing cycles resulted in a final dyestuff concentration of 0.066 g l^{-1} (0.042 mM) and a final Mg^{2+} concentration of 1.63 mM. Symbols (■) represent an experiment where the dyestuff aggregation has been initiated by hand mixing of the two components, whereas symbols (○) represent an experiment where the components were mixed by means of an SF-20 stopped-flow device.

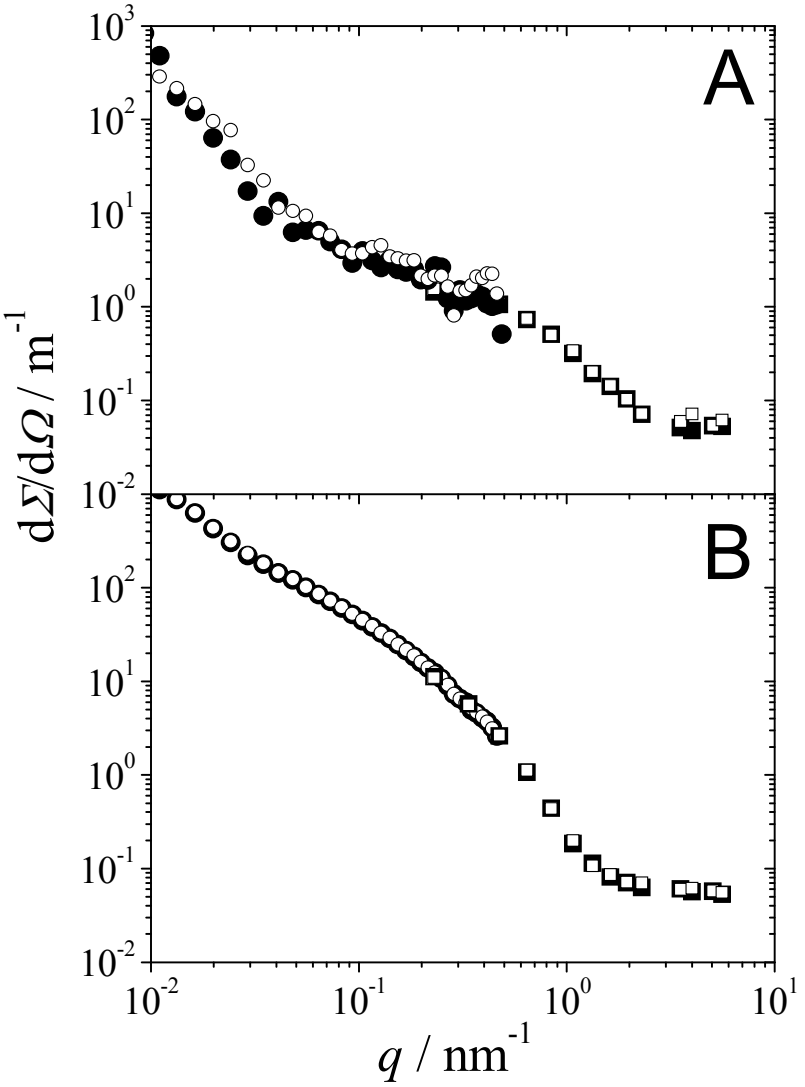

Figure S2. Scattering curves from shots with the SF-400 stopped flow device. All shots were performed with equal dyestuff and alkaline earth concentrations (c_{dye} = 0.33 g l^{-1}, $[Ba^{2+}]$ = 1.6 mM) but at different detector distances of 1 m (symbols □,■) and of 10 m (symbols ○,●). Graph (A) shows scattering curves which were calculated by averaging three single curves recorded at t = 25, 55 and 85 ms, respectively, thus representing an averaged time after initiation of t = 55 ms. Graph (B) shows scattering curves which were calculated by averaging 20 single curves recorded in between t = 1,5 s and t = 2,1 s, respectively, thus representing an averaged time after initiation of t = 1,8 s. The results illustrate (i) a good reproducibility of the shots achieved with the SF-400 stopped-flow instrument and (ii) justify the combination of time-resolved averaged scattering recorded at different detector distances.

Modeling of Small-Angle Scattering Data by Means of the Cylinder Model

The small angle x-ray scattering from samples was interpreted by means of the cylinder model. The form factor of a homogeneous cylinder with length L and cross section radius R is given by[1]:

$$P_{\mathrm{cyl}}(q,L,R) = \frac{\mathrm{d}\Sigma/\mathrm{d}\Omega(q)_{\mathrm{cyl}}}{\mathrm{d}\Sigma/\mathrm{d}\Omega(q=0)_{\mathrm{cyl}}} = \int_0^{\pi/2} \left[\frac{2J_1(qR\sin(x))}{qR\sin(x)} \frac{\sin(qL\cos(x)/2)}{qL\cos(x)/2}\right]^2 \sin(x)dx \qquad \text{(SI-1)}$$

In the present work, we added a polydispersity to the cylinder cross-section in terms of a Gaussian distribution of the radius R' around its mean value R with absolute standard deviation σ and relative standard deviation σ/R. Moreover, a q independent background scattering was included into the model. Accordingly, model scattering intensities of cylinders with polydisperse cross-sections were calculated as

$$I_{\mathrm{poly}}(q,L,R,\sigma) = \frac{I_0}{\sqrt{2\pi\sigma^2}} \int_{R'} \exp\left(-\frac{(R'-R)^2}{2\sigma^2}\right) P_{\mathrm{cyl}}(q,L,R')\, dR' + bg \quad , \qquad \text{(SI-2)}$$

where I_0 represents the scattering intensity at zero momentum transfer and bg is the background scattering.

Cylinder Radii Obtained from Guinier Fits

The scattering intensity of cylindrical structures with length L and radius R is proportional to q^{-1} within the regime $qL > 1$ and $qR < 1$. This can be utilized to determine R by means of a Guinier[1] analogous approximation:

$$q \cdot \frac{\mathrm{d}\Sigma}{\mathrm{d}\Omega}(q)\Big|_{qR<1} \approx A \cdot \exp\left(-\frac{q^2R^2}{6}\right) \quad . \qquad \text{(SI-3)}$$

Besides modeling the experimental data with cylinder form factors based on eq SI-2, eq SI-3 represents an alternative for the determination of R. As indicated in Figure S3-B, the values resulting for R from both of these alternative methods agree within experimental uncertainty.

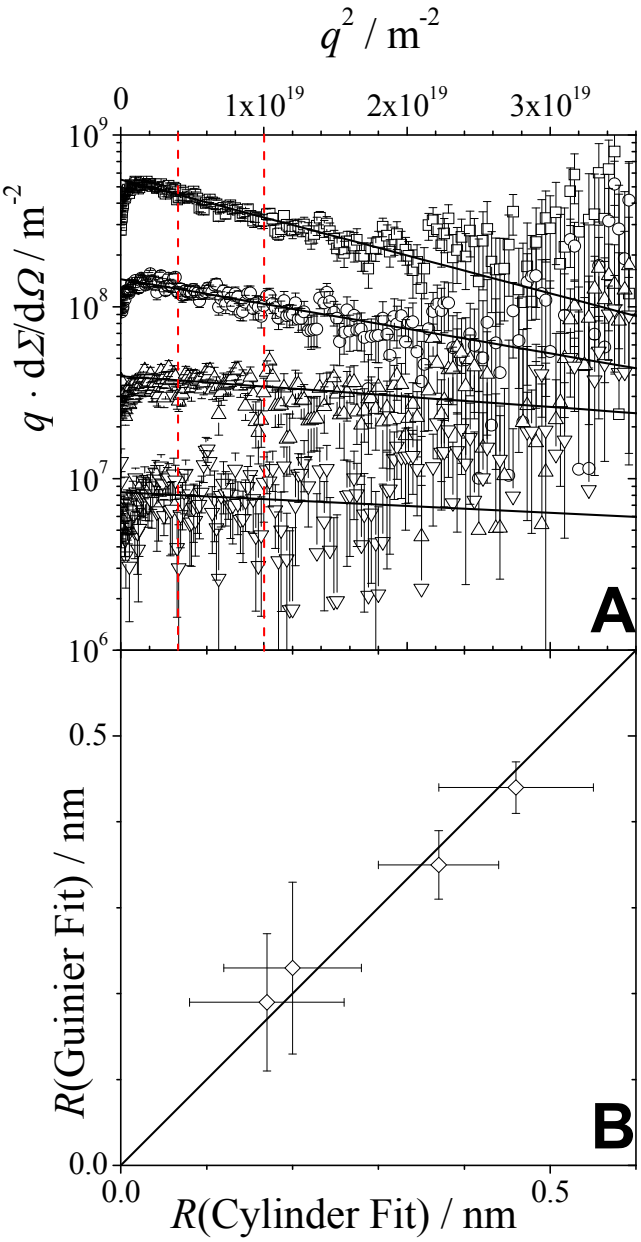

Figure S3. (A) Plots of the product of the scattering vector q with the SAXS of aqueous solutions containing 0.66 g l^{-1} (□), 0.33 g l^{-1} (○), 0.17 g l^{-1} (△) and 0.08 g l^{-1} (▽) mixed RD and YD in stoichiometric ratio (cf. Figure 3A in the manuscript). The continuous lines represent Guinier fits according to eq SI-3. For these fits, only the q regime in between the red dashed lines was considered. For the sake of clarity, the curves are separated from each other by a factor of 2, respectively. (B) Comparison of the R values resulting from cylinder fits (eq SI-2, cf. Table 2 in the manuscript) with the R values resulting from Guinier fits (eq SI-3).

Parameter Distortion Based on an Interpretation of the Scattering of a Mixture of Small and Large Cylinders by Means of the Form Factors of the Large Cylinders

The scattering of matured dyestuff fibres is modeled by means of form factors of cylinders with a length of L = 200 nm and variable scale (I_0) and radius (R). This interpretation does not consider possible smaller species with a size in the regime of 10 nm (e.g. unconsumed building units) that might coexist with the large aggregates. Whereas the presence of such species hardly affects the low q regime of the total scattering, it may influence significantly the scattering intensity in the q regime of the cylinder cross section and thus distort the values of the fitting parameter R. In order to scrutinize such an influence, we calculated theoretical scattering curves of a bimodal system consisting of large cylinders with lengths of L_1 = 200 nm and small cylinders with length L_2 = 10 nm and radius R_2 = 0.5 nm. Initially the large cylinders have a radius of R_2 = 4 nm and the ratio of total volume occupied by small cylinders to the total volume occupied by large ones is V_2/V_1 = 4:1 (Figure S4, lower left). Then the large cylinders grow laterally by incorporation of the small ones until the volume ratio has reduced to V_2/V_1 = 1:4 (Figure S4, upper right). In the course of the incorporation of small cylinders into large ones, the total volume of the latter has thus increased by a factor of 4, corresponding to an increase of the radius of the latter from R_2 = 4 to R_2 = 8 nm (Note that L_2 remains unaffected). Theoretical scattering curves I_{theor} of several intermediate states in the range of 4:1 ≥ V_2/V_1 ≥ 1:4 were calculated using the cylinder form factor[1] P_{cyl} as given by eq SI-1:

$$I_{\text{theor}} = V_1 R_1^2 L_1 P_{\text{cyl}}(R_1, L_1) + V_2 R_2^2 L_2 P_{\text{cyl}}(R_2, L_2) \qquad \text{(SI-4)}$$

For all calculations, a polydispersity of cylinder cross-sections of σ/R = 0.33 has been included in terms of eq SI-2. Subsequently, the theoretical scattering curves have been fitted by means of eq SI-2, i.e. by excluding the small cylinders from the fitting function. During fitting, L_2 = 200 nm and σ/R_2 = 0.33 were kept constant and R_2 and I_0 were adjusted. For each fitted curve, a quantity proportional to the product of mass concentration and mass per unit length of the cylinders has been established (see eq SI-2) and plotted versus the corresponding fitted cylinder radius. The resulting correlation is compared with the exact correlation in Figure S4.

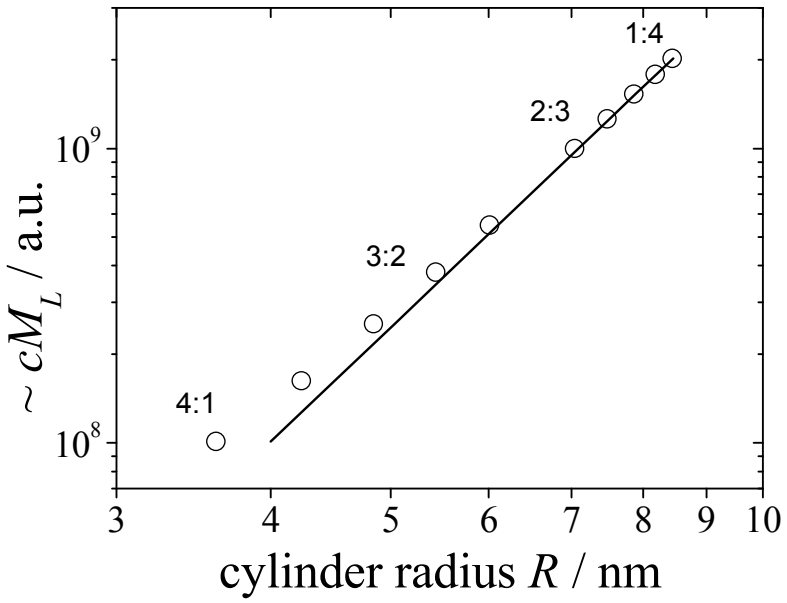

Figure S4. The theoretical correlation of the product of mass concentration c and mass per unit length M_L of a cylinder with its Radius R is represented by the continuous line ($cM_L \sim R^4$). The symbols (○) illustrate values of cM_L and R obtained by the fit procedure described above. The graph illustrates that the deviations of the fitted values from the correct ones represented by the continuous line are negligible.

Estimation of the Dyestuff Concentration within Centrifuged Dyestuff Gels

Figure S5 exemplifies a sample used for ASAXS and x-ray absorption measurements. In order to estimate the metal-to-dye stoichiometry of the formed aggregates situated in the gel phase at the bottom of the capillary, both the Sr^{2+} concentration within the gel, $[Sr^{2+}]_b$, and the concentration of Sr^{2+} ions that bind specifically to the dye within the gel, $[Sr^{2+}]_{spec}$, have to be determined. It is important to note that the latter may be significantly smaller than $[Sr^{2+}]_b$, since a large fraction of the gel phase might consist of aqueous Sr^{2+} solution, i.e. the gel might contain many Sr^{2+} ions that do not contribute to $[Sr^{2+}]_{spec}$. Whereas $[Sr^{2+}]_b$ is accessible by absorption measurements, $[Sr^{2+}]_{spec} \leq [Sr^{2+}]_b$ can only be determined by measuring ASAXS at the bottom position of the capillary (see ref. 2 and manuscript). Once $[Sr^{2+}]_{spec}$ is determined, only the dyestuff concentration at the bottom position, $c_{dye\text{-}b}$, is needed in order to establish the desired metal-to-dye stoichiometry of the formed aggregates. $c_{dye\text{-}b}$ can be estimated if the following two

prerequisites are fulfilled: (i) the entire dyestuff has to be located at the bottom domain and (ii) the Sr^{2+} concentrations within the two domains of the capillary have to be homogeneous in z-direction. Condition (i) is adequately fulfilled since the top domain is colorless. Besides, the obvious stability of the gel-like phase is in support of its homogeneity: After a short period of centrifugation, positions, shapes and colors of the bottom domains became invariant to further mechanical stress.

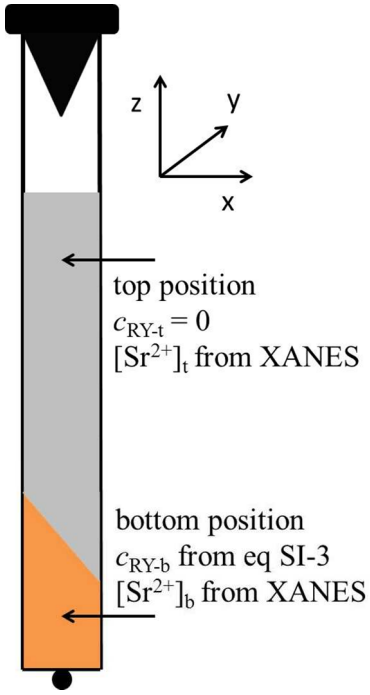

Figure S5. Schematic of a quartz capillary containing RD and YD in a 1:1 molar ratio as well as an excess of $SrCl_2$. The excess of Sr^{2+} ions causes an immediate aggregation process by which the entire ensemble of RD and YD molecules is consumed. The formed aggregates can be separated from the remaining solution by centrifugation such that they form a gel-like domain located at the bottom of the capillary. The remaining solution thereby becomes colorless, indicating that the dyestuff concentration within the supernatant is close to zero. Provided that the Sr^{2+} concentrations within the gel, $[Sr^{2+}]_b$, and within the supernatant, $[Sr^{2+}]_t$, do not change with the z-coordinate, respectively, they can be determined by measuring x-ray absorption spectra at the top and the bottom position of the capillary.

We denote the total dyestuff and total Sr^{2+} concentrations within the sample as c_{dye} and $[Sr^{2+}]$, respectively, and use the denotations given in Figure S5 for the respective concentrations at top (t) and bottom (b) position. Successively we can write

$$c_{\mathrm{dye}} = c_{\mathrm{dye-b}} \frac{V - V_{\mathrm{t}}}{V}, \quad \text{therefore} \quad c_{\mathrm{dye-b}} = c_{\mathrm{dye}} \frac{V}{V - V_{\mathrm{t}}} \quad , \tag{SI-5}$$

where V is the total sample volume. The volume of the top domain, V_{t}, can be expressed considering

$$[\mathrm{Sr}^{2+}]V = [\mathrm{Sr}^{2+}]_{\mathrm{t}} V_{\mathrm{t}} + [\mathrm{Sr}^{2+}]_{\mathrm{b}} (V - V_{\mathrm{t}}), \quad \text{therefore} \quad V_{\mathrm{t}} = V \frac{[\mathrm{Sr}^{2+}] - [\mathrm{Sr}^{2+}]_{\mathrm{b}}}{[\mathrm{Sr}^{2+}]_{\mathrm{t}} - [\mathrm{Sr}^{2+}]_{\mathrm{b}}} \quad . \tag{SI-1}$$

Introducing eq SI-1 into eq SI-5 cancels the total sample volume V and yields the following expression for the desired dyestuff concentration within the bottom domain.

$$c_{\mathrm{dye-b}} = c_{\mathrm{dye}} \frac{[\mathrm{Sr}^{2+}]_{\mathrm{b}} - [\mathrm{Sr}^{2+}]_{\mathrm{t}}}{[\mathrm{Sr}^{2+}] - [\mathrm{Sr}^{2+}]_{\mathrm{t}}} \tag{SI-2}$$

Calculation of Sr^{2+} Concentrations from X-Ray Absorption Spectra

The strontium-K-edge at ~16105 eV was used to quantify the Sr^{2+} concentrations $[Sr^{2+}]_t$ and $[Sr^{2+}]_b$ at the top and the bottom positions of the ASAXS samples, respectively. The mass density ρ of the absorbing species can be written as the derivative of the absorption coefficient μ with respect to the specific absorption cross-section σ.

$$\rho = \frac{\mathrm{d}\mu}{\mathrm{d}\sigma} \approx \frac{\Delta\mu}{\Delta\sigma} = \frac{\Delta(\mu \cdot d)}{d \cdot \Delta\sigma} \tag{SI-4}$$

In eq SI-4, d is the sample thickness. An example of an x-ray absorption spectrum is given in Figure S6. X-ray absorption spectroscopy yields the product μd as a function of the photon energy E. The product $\mu d = \ln(I_0/I)$ is calculated from the intensities of the primary beam (I_0) and of the beam after transmitting the sample (I). As illustrated in Figure S6, the difference $\Delta(\mu d)$ can be determined by fitting a spline to the pre-edge data and to the post-edge data, respectively. We chose a function of the empirical form[2] a/E^3 for the pre-edge spline, where a is a constant. The post-edge data was then fitted with the same spline plus $\Delta(\mu d)$, where $\Delta(\mu d)$ was chosen such that the areas A_1 and A_2 caused by the near-edge fine structure became equal. The edge difference in specific absorption cross-section, $\Delta\sigma$, was estimated by choosing a pre-edge data pair (σ_1, E_1) and a post-edge data pair (σ_2, E_2) from tabulated[3] values.

$$\Delta\sigma \approx \frac{\sigma_2 E_2^3 - \sigma_1 E_1^3}{E_{\text{edge}}^3} \qquad \text{(SI-5)}$$

With $\Delta(\mu d)$ from the experimental data and $\Delta\sigma$ from eq SI-5, the mass density ρ corresponding to the mass concentration of Sr^{2+} is accessible via eq SI-4. The molar concentrations of Sr^{2+} is then calculated as $[Sr^{2+}] = \rho/M_{Sr}$, where M_{Sr} is the molar mass of strontium.

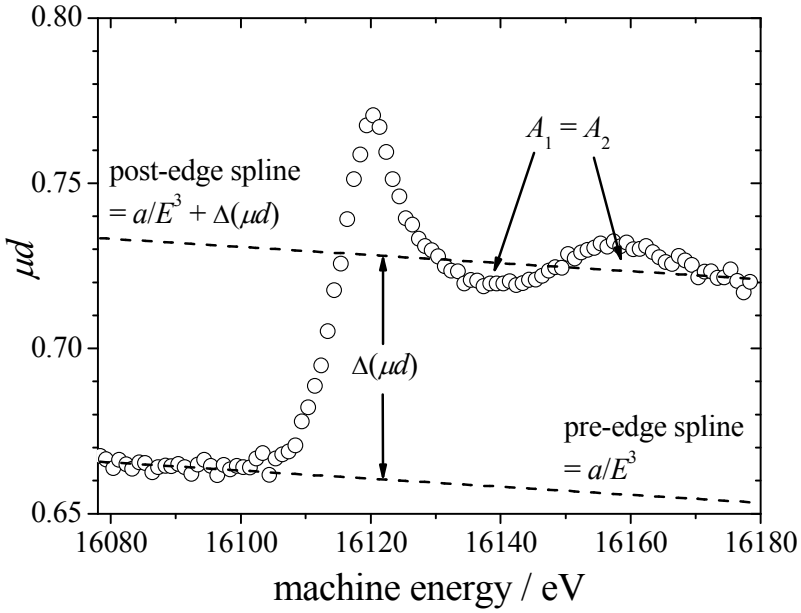

Figure S6. Illustration of an x-ray absorption spectrum used to determine the jump in absorption at the strontium-K-edge (E_{edge} = 16105 eV). The machine energy displayed by the abscissa deviates by about 8 eV from the real photon energy due to uncertainties of the monochromator control.

Direct Comparison of the SAXS from Samples Used for SAXS and ASAXS Experiments

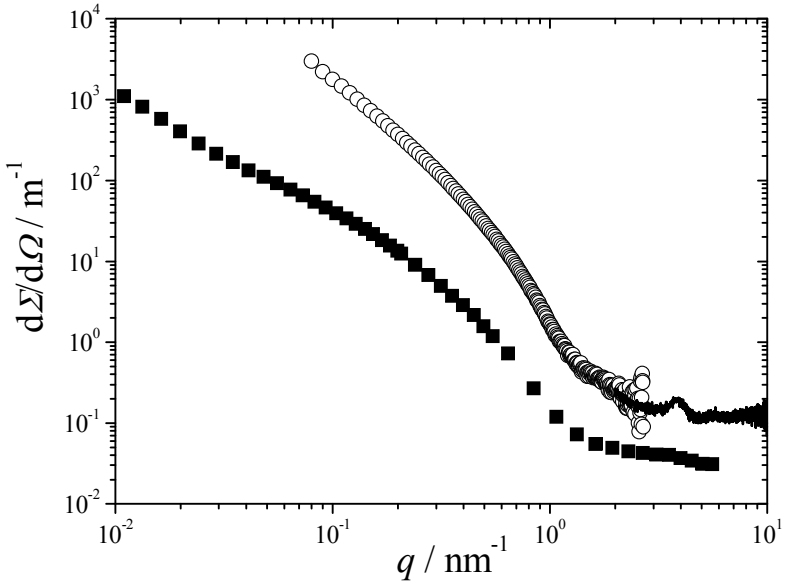

Figure S7. Comparison of the SAXS from a dyestuff gel (○ and continuous line at high q) containing approximately 11.3 g l^{-1} dyestuff (see Table 3 in the manuscript) with the scattering from a sample containing 0.33 g l^{-1} dyestuff (■). Both samples contain an excess of Sr^{2+} ions with respect to the anionic dyestuff charges and represent a temporally stable state of matured dyestuff aggregates.

References.

1. Guinier, A.; Fournet, G. Small-Angle Scattering of X-Rays. John Wiley and Sons: New York, 1955.
2. Stuhrmann, H. B. Resonance Scattering in Macromolecular Structure Research. *Adv. Polym. Sci.* **1985**, *67*, 123-163.
3. McMaster, W. H.; Kerr Del Grande, N.; Mallett, J. H.; Hubbell, J. H. Compilation of X-Ray Cross Sections. *Lawrence Livermore National Laboratory Report* **1969** UCRL-50174 Section II Revision I.